



Article

# Ultrastructural Analysis of *Prune Dwarf Virus* Intercellular Transport and Pathogenesis

Edmund Koziel <sup>1</sup> , Katarzyna Otulak-Koziel <sup>1,\*</sup> and Józef J. Bujarski <sup>2,3</sup>

<sup>1</sup> Faculty of Agriculture and Biology, Department of Botany, Warsaw University of Life Sciences—SGGW, Nowoursynowska Street 159, 02-776 Warsaw, Poland; edmund\_koziel@sggw.pl

<sup>2</sup> Department of Biological Sciences, Northern Illinois University, DeKalb, IL 60115, USA; jbjarski@niu.edu

<sup>3</sup> Institute of Bioorganic Chemistry, Polish Academy of Sciences, Noskowskiego 12/14, 61-704 Poznań, Poland

\* Correspondence: katarzyna\_otulak@sggw.pl; Tel.: +48-(22)5-932-657

Received: 5 August 2018; Accepted: 28 August 2018; Published: 29 August 2018



**Abstract:** *Prune dwarf virus* (PDV) is an important viral pathogen of plum, sweet cherry, peach, and many herbaceous test plants. Although PDV has been intensively investigated, mainly in the context of phylogenetic relationship of its genes and proteins, many gaps exist in our knowledge about the mechanism of intercellular transport of this virus. The aim of this work was to investigate alterations in cellular organelles and the cell-to-cell transport of PDV in *Cucumis sativus* cv. Polan at ultrastructural level. To analyze the role of viral proteins in local transport, double-immunogold assays were applied to localize PDV coat protein (CP) and movement protein (MP). We observe structural changes in chloroplasts, mitochondria, and cellular membranes. We prove that PDV is transported as viral particles via MP-generated tubular structures through plasmodesmata. Moreover, the computer-run 3D modeling reveals structural resemblances between MPs of PDV and of *Alfalfa mosaic virus* (AMV), implying similarities of transport mechanisms for both viruses.

**Keywords:** viral intercellular transport; immunolocalization; plasmodesmata; 3D protein structure; *Prune dwarf virus*

## 1. Introduction

The *Bromoviridae* are a large family of plant RNA viruses which include many economically important pathogens of monocots and dicots [1]. The family contains 6 genera, with one of most interesting being the genus *Ilarvirus*. Amongst the *Ilarviruses*, an important species is *Prune dwarf virus* (PDV) [2,3]. This viral pathogen infects a whole range of hosts from plum, sweet cherry, and peach to various test plants [4,5]. The genome of PDV, like other *Ilarviruses*, is multipartite and consists of 3 viral RNA (vRNA) molecules: RNA1, RNA2 and RNA3 [1,6]. RNA1 and RNA2 encode two replication proteins, the “replicase” (P1 protein) and RNA-dependent RNA polymerase (RdRp, P2 protein), respectively [7,8]. Both P1 and P2 are required for replication of vRNAs and build replication complexes during viral infection [1,9]. RNA3 encodes two proteins, the movement protein (MP) and coat protein (CP) [6]. PDV-MP is involved in cell-to-cell transport [5,6]. Apart from forming the viral capsid, PDV-CP is needed for genome activation, and possibly also for cell-to-cell transport [5,6,10]. Our previous microscopic and bioinformatics studies showed that PDV infection induces changes in cell membranes and its cell-to-cell transport, likely similar to *Alfalfa mosaic virus* (AMV) [11,12]. This study focuses on sequential ultrastructural changes in cell organelles and PDV-induced structures in cucumber plants. Moreover, the study shows the potential mechanism of PDV intercellular transport based on both microscopic and bioinformatic analyses. Our observations reveal changes in chloroplasts, mitochondria and endomembranes, as well as in the cell wall and plasmodesmata, the latter carrying tubular structures for virus translocation.

## 2. Results

### 2.1. Symptomatology Induced by Prune Dwarf Virus (PDV) in *Cucumis sativus*

The first morphological changes induced by PDV were observed approximately seven days post-inoculation (dpi). At this stage, we observed chlorotic spots on the inoculated cotyledons (Figure 1A). From 14 dpi we also observed characteristic alterations of upper leaves (black frame on Figure 1A). From this point, the viral infection reached systemic leaves. Frequently, leaves of infected cucumber were deformed, chlorotic with yellowing veins (Figure 1B). On the other hand on some leaves, alterations at 14 dpi were slightly different, without deformations but instead with yellowing leaf blades along the edges (Figure 1C). Mock-inoculated plants did not develop symptoms on cotyledons and the leaves (Figure 1D).

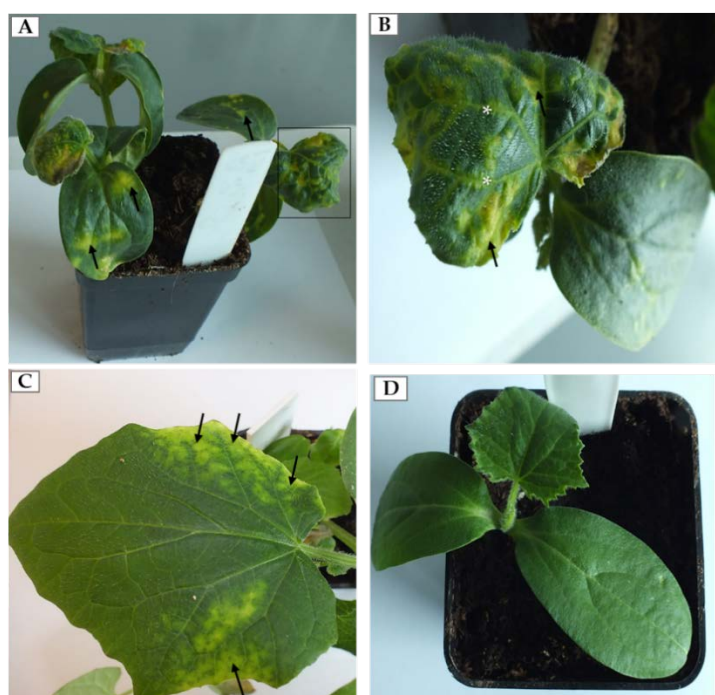


**Figure 1.** Morphological alterations of infection caused by *Prune dwarf virus* (PDV) on cucumber. (A) Chlorotic spots (arrow) on the cotyledons and leaves of cucumber infected by PDV (14 dpi). The black frame area is enlarged in (B); (B) Enlarged deformed leaf with chlorotic spots (arrow) and yellowing veins (\*); (C) Yellowing of leaf blades along the edges (arrow) at 14 dpi; (D) Mock-inoculated cucumber plants without symptoms (14 dpi).

### 2.2. Immunofluorescence Localization of Coat Protein (CP) in PDV-Infected Cucumber Leaves

In order to choose which cell types to analyze by detailed TEM (transmission electron microscope) and double-immunogold labeling, we initially performed immunofluorescence labeling of PDV-CP to localize viral particles inside specific cells and types of tissue inside the cucumber leaf. At 14 dpi, PDV-CP was localized in various tissues with different frequency in the individual leaf parts. Most commonly, the occurrence of CP was observed in the stomata, palisade and spongy mesophyll cells (Figure 2A,B). Moreover, in the infected leaves, the deformations were visible in spongy mesophyll cells (Figure 2B). Presence of CP was also confirmed in the central vascular bundle in the main vein, confirming systemic infection (Figure 2C). The presence of PDV-CP was noticed in both xylem and phloem parenchyma (Figure 2C). No deformations and PDV-CP localization are shown (Figure 2D).

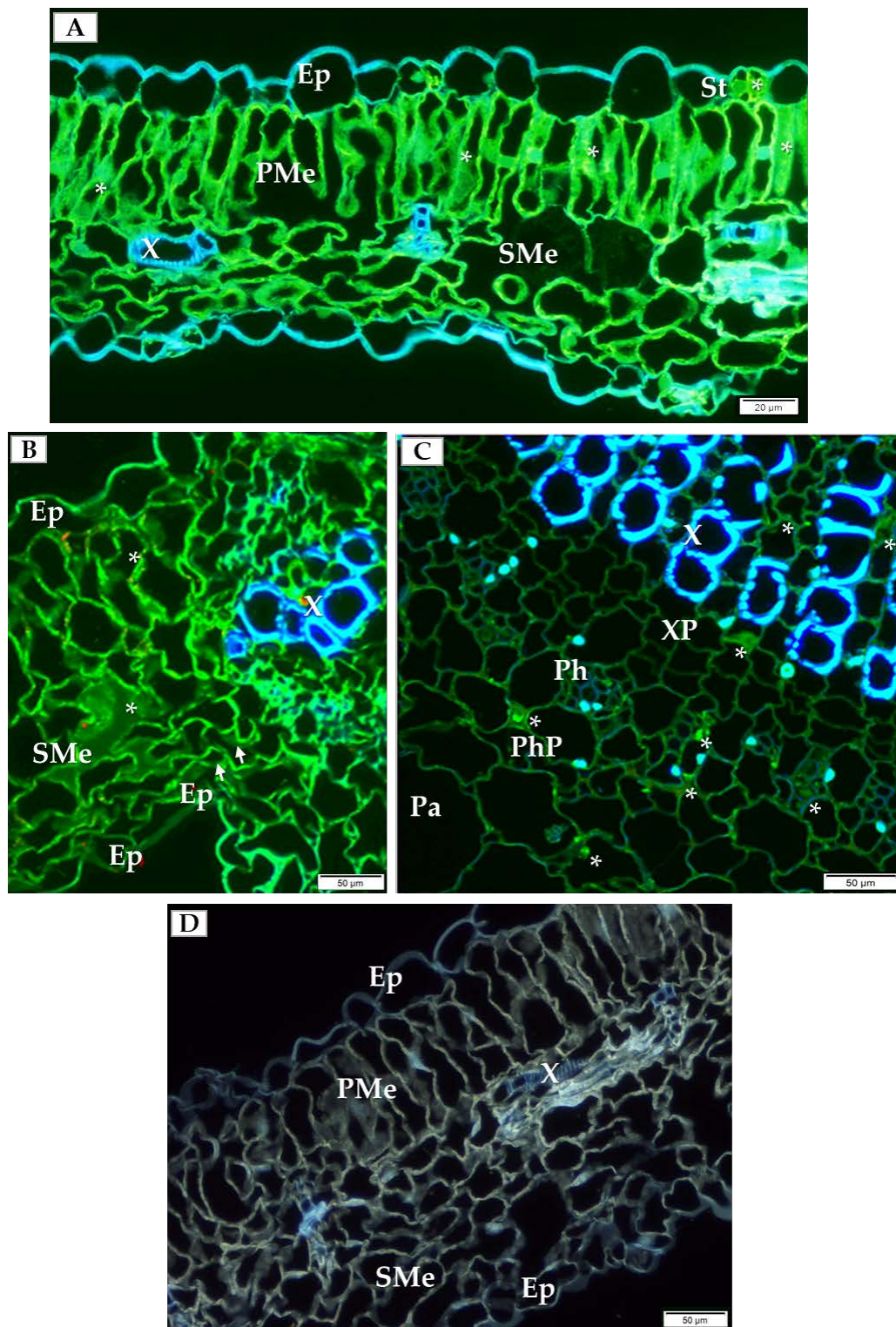


**Figure 2.** Immunofluorescence localization of PDV-coat protein (PDV-CP) epitopes in the infected cucumber leaf tissue of *Polan* variety (14 dpi). (A) Localization of the epitopes of PDV-CP (green fluorescence, marked with \*) in stomata and palisade mesophyll cells (14 dpi), Bar 20  $\mu\text{m}$ ; (B) PDV-CP epitope (\*) inside spongy mesophyll (14 dpi). Deformations of cell wall in spongy mesophyll cell are marked with white arrows, Bar 50  $\mu\text{m}$ ; (C) Cross section of cucumber leaf through main vein with presence of CP (\*) in xylem and phloem parenchyma (14 dpi), Bar 50  $\mu\text{m}$ ; (D) Section of mock-inoculated leaf without PDV-CP, Bar 50  $\mu\text{m}$ . Abbreviations: Ep—epidermis, St—stomata, PMe—palisade mesophyll, SMe—spongy mesophyll, Pa—parenchyma, X—tracheal element, XP—xylem parenchyma, Ph—phloem, PhP—phloem parenchyma.

### 2.3. Ultrastructural Alterations in Cucumber Cells During PDV Infection

Sequential changes in the structure of some crucial plant cell organelles were found in the infected cucumber leaves. Most significantly, the electron translucent regions appeared in the stroma between thylakoids in chloroplasts of spongy mesophyll cells (Figure 3A,B). Moreover, the outer membranes of disintegrated chloroplasts and deformed thylakoids were observed in the cytoplasm of these cells that often also had irregular and deformed cell walls (Figure 3C). Such changes were not observed in chloroplasts from mock-inoculated cucumber plants (Figure 3D). On the other hand, altered mitochondria were mainly observed inside companion cells of the phloem; these cells contained many viral particles and showed the enlarged endoplasmic reticulum (ER) cisterns (Figure 3E) and different stages of other mitochondrial alterations (Figure 3F,G). Many mitochondria had reduced cristae and large electron translucent regions within the mitochondrial matrix (Figure 3F). When the companion cell was filled with PDV particles the mitochondrial cristae completely disappeared (Figure 3G).

Another type of cellular changes was associated with the generation of membranous structures in infected cells. In palisade mesophyll cells that contained viral particles, the enlarged ER and vesicle pockets were visible inside the vacuoles (Figure 4A). Simultaneously in mesophyll cells, we observed spherules (vesicles with viral particles on their surface) (Figure 4B). Similar changes were noticed inside companion cells (Figure 4C), where many spherules and viral particles were found (Figure 4D).

PDV infection also affected the plasmodesmata, especially in mesophyll cells that had PDV particles (Figure 5A). Namely, the plasmodesmata kept the tubular structures that passed through cell wall (Figure 5B), and the tubular structures frequently carried the intact PDV particles (Figure 5C).

We have also clearly confirmed the connections between tubular structures and viral particles in transverse sections of plasmodesmata (Figure 6A). In many cases, viral particles could be observed inside tubules which pass through plasmodesmata of more than two cells (Figure 6B). Frequently near the cell wall, the enlarged ER could be observed (Figure 6C). Viral particles were found near the secondary plasmodesmata (Figure 6D). Changes in the plasmodesmata structure paralleled alterations in the cell wall, especially in the phloem parenchyma that had many cell wall invaginations (arrow, Figure 7A) or irregular structures (Figure 7B). Such irregularities were not observed in uninfected cells. In case of cells with irregular cell walls, the plasmalemma was often invaginating in many regions (Figure 7B). In some cells with irregular wall structures, we observed the presence of viral particles inside the vacuole (Figure 7C), with the vacuolar lumen having connections to cytoplasm (Figure 7C). Alterations near the cell wall were also observed in the companion cells and sieve tubes. The cell wall around plasmodesmata was thicker whereas in companion cells numerous viral particles were observed (Figure 7D).

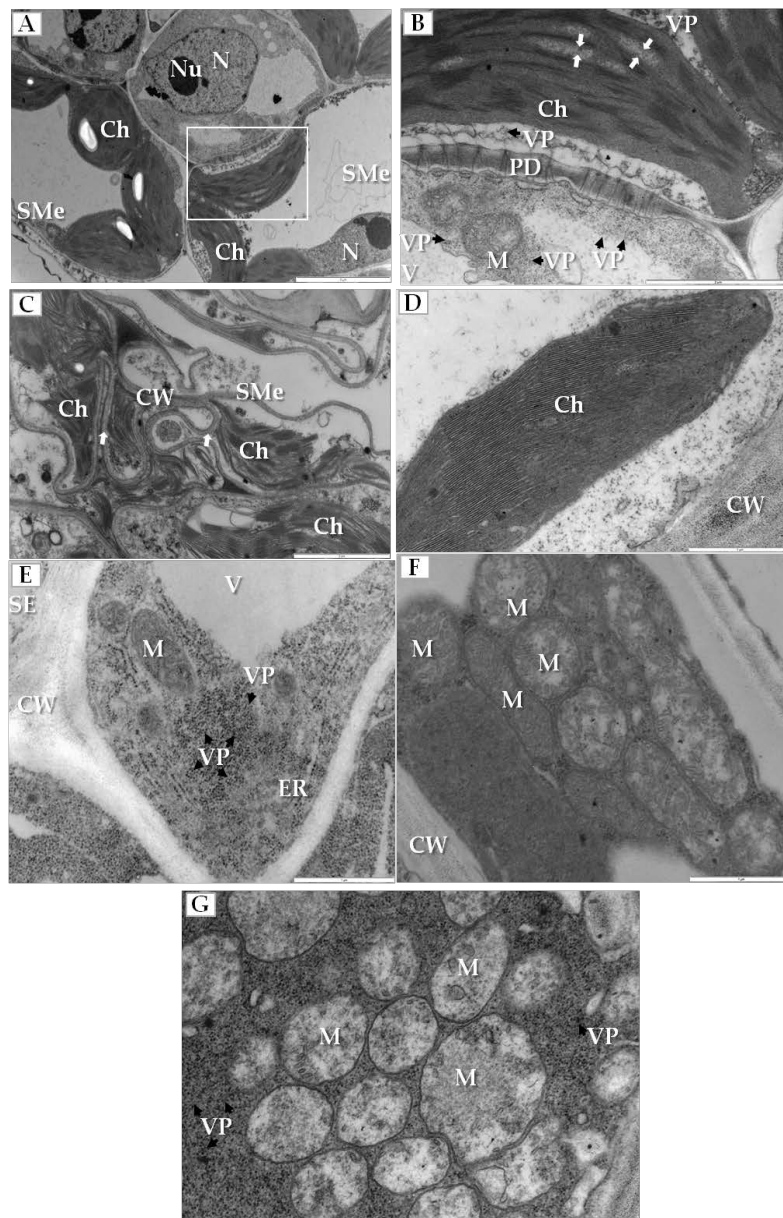


**Figure 3.** Ultrastructural alterations in cucumber organelles and cell wall during PDV infection. (A) Section through the PDV-infected leaf blade, with spongy mesophyll cells with changed chloroplasts. The white framed area is enlarged in (B), Bar 5  $\mu\text{m}$ ; (B) Spongy mesophyll cell from (A) with electron translucent regions in the stroma between thylakoids (white arrow) and also with viral particles present (VP, black arrow), Bar 2  $\mu\text{m}$ ; (C) Altered spongy mesophyll cell from infected cucumber with disintegrated chloroplasts and the cell wall irregular and deformed (white arrow), Bar 2  $\mu\text{m}$ ; (D) Parenchyma cell of from mock-inoculated cucumber without altered chloroplast and cell wall, Bar 1  $\mu\text{m}$ ; (E) Companion cell from infected cucumber with enlarged endoplasmic reticulum cisterns and the PDV particles present in cytoplasm (VP, black arrow), Bar 1  $\mu\text{m}$ ; (F) Fragment of a companion cell from infected cucumber showing mitochondria with reduced cristae and large electron translucent regions- early stage of mitochondrial changes, Bar 1  $\mu\text{m}$ ; (G) Region in the cytoplasm of a companion cell filled with PDV particles (VP, black arrow), and with no cristae in the mitochondria, Bar 1  $\mu\text{m}$ . Abbreviations: SMe—spongy mesophyll, SE—sieve tube, Ch—chloroplast, N—nucleus; Nu—nucleolus, PD—plasmodesmata, V—vacuole, M—mitochondrion, CW—cell wall, ER—endoplasmic reticulum, VP, black arrow—viral particles.

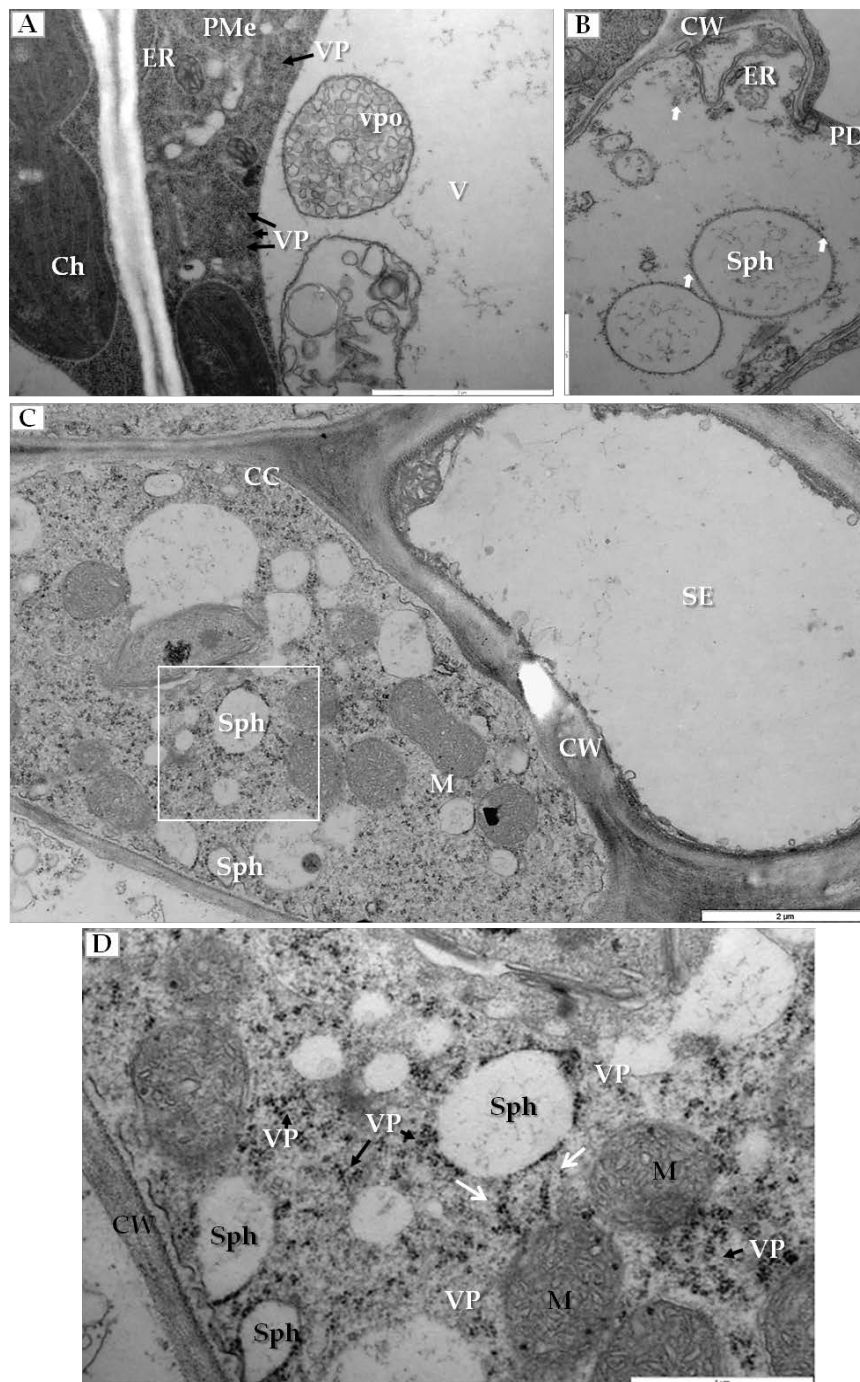


**Figure 4.** Membranous structures induced by PDV infection. (A) Fragment of palisade mesophyll cell from PDV infected cucumber with viral particles (VP, black arrow) in cytoplasm and vesicle pockets inside vacuole, Bar 2  $\mu\text{m}$ ; (B) Mesophyll cell with spherules carrying viral particles on the surface (white arrow), Bar 1  $\mu\text{m}$ ; (C) Section through a phloem cell with companion cell and sieve tube, showing various numbers of membranous structures and spherules. The white frame area is enlarged in (D), Bar 2  $\mu\text{m}$ ; (D) A fragment of companion cell with viral particles present, arranged in line (white arrow) connected to the spherule, Viral particles in cytoplasm (black arrow) Bar 1  $\mu\text{m}$ . Abbreviations: PMe—palisade mesophyll, SE—sieve tube, Ch—chloroplast, PD—plasmodesmata, vpo—vesicle pockets, Sph—spherules V—vacuole, M—mitochondrion, CW—cell wall, ER—endoplasmic reticulum, VP, black arrow—viral particles.

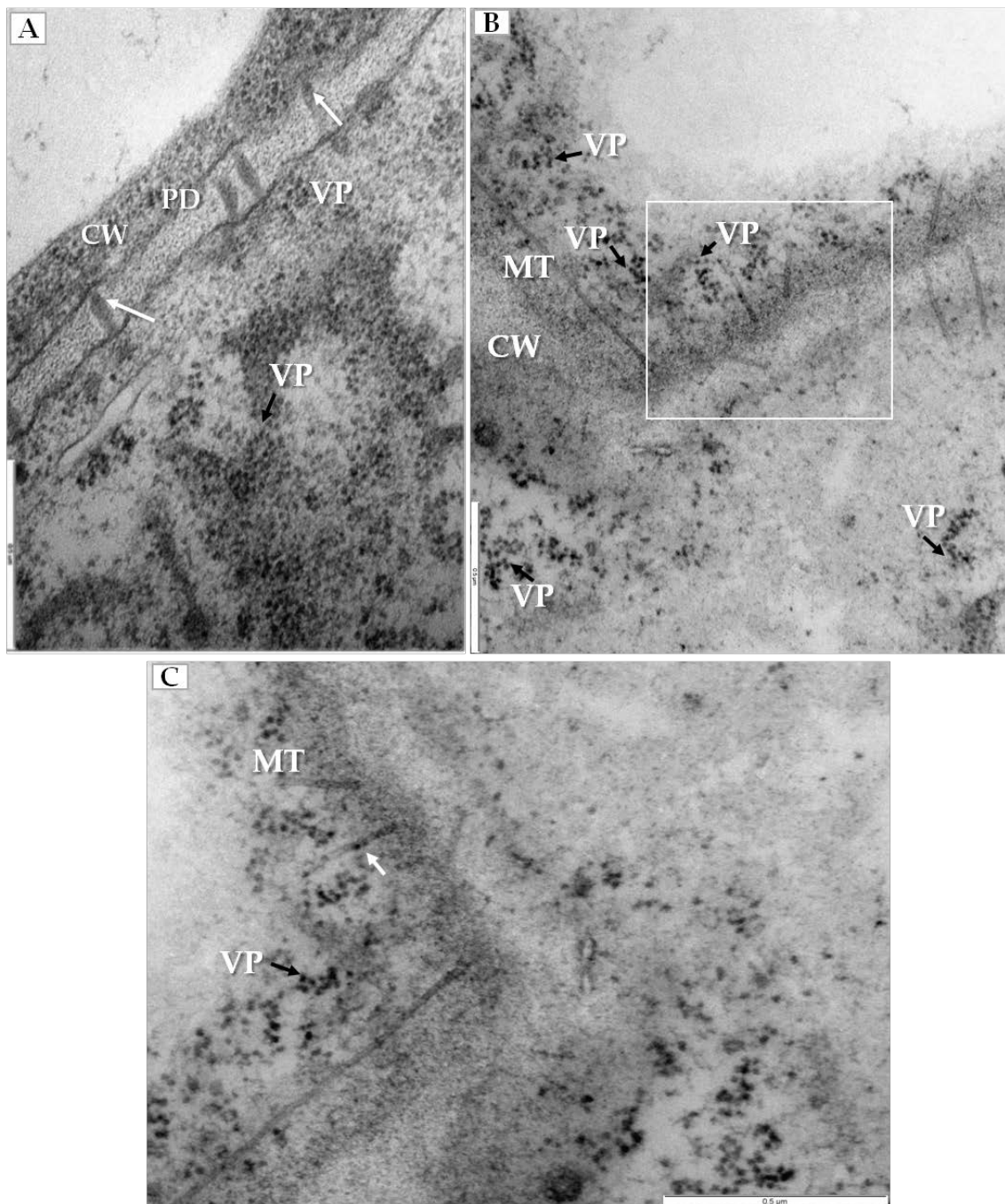


**Figure 5.** Changes in plasmodesmata in PDV-infected cucumber leaf. **(A)** Section of mesophyll cell with extended plasmodesmata and viral particles (VP, black arrow). Viral particles present inside plasmodesmata and indicated with a white arrow, Bar 0.5 μm; **(B)** Fragment of mesophyll cell containing viral particles (VP, black arrow) near tubular structures induced by PDV-MP. The white frame area is presented in **(C)**, Bar 0.5 μm; **(C)** This enlarged fragment of infected mesophyll cell shows viral particles inside tubular structures induced by PDV MP (white arrow). Viral particles (VP) in cytoplasm near plasmodesmata are marked with black arrow, Bar 0.5 μm. Abbreviations: CW—cell wall, PD—plasmodesmata, MT—movement protein induced tubular structures, VP, black arrow—viral particles.

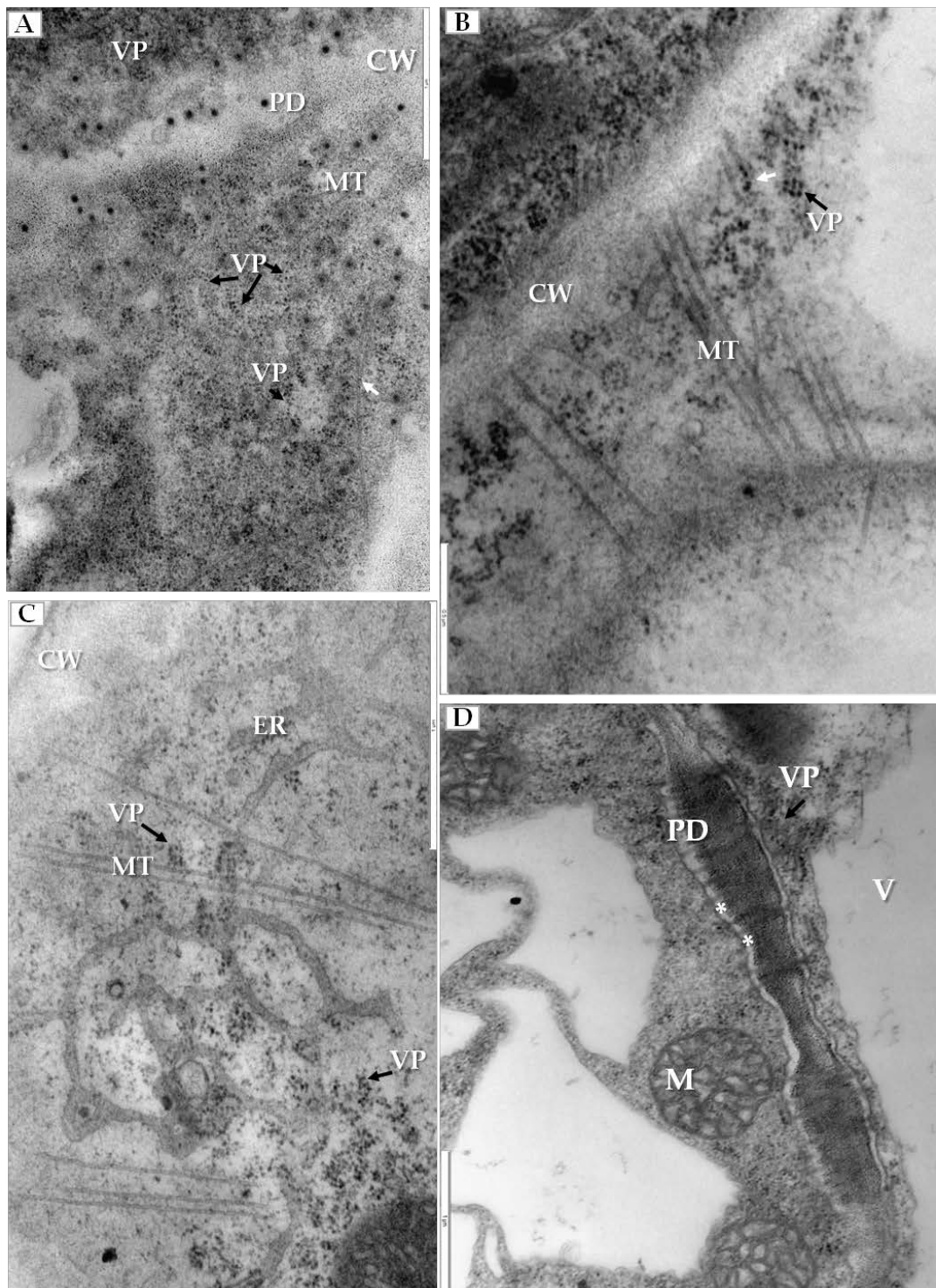


**Figure 6.** Tubular structures and changes in secondary plasmodesmata in PDV infected cucumber plants. (A) Phloem parenchyma cell with transverse sections of plasmodesmata. Viral particles are visible in cytoplasm (VP, black arrow) and in tubular structures directed to plasmodesmata (white arrow), Bar 1  $\mu\text{m}$ ; (B) Tubular structures with viral particles inside (white arrow). Tubular structures pass through cell walls of three cells. Viral particles (VP, black arrow) near plasmodesmata, Bar 0.5  $\mu\text{m}$ ; (C) PDV particles (VP, black arrow), tubular structures and enlarged endoplasmic reticulum cisterns in phloem parenchyma cell, Bar 1  $\mu\text{m}$ ; (D) Viral particles (VP, black arrow) near secondary plasmodesmata in phloem parenchyma cell. Moved plasmalemma (\*) near secondary plasmodesmata, Bar 1  $\mu\text{m}$ . Abbreviations: CW—cell wall, PD—plasmodesmata, ER—endoplasmic reticulum, MT—movement protein induced tubular structures, VP, black arrow—viral particles, M—mitochondrion; V—vacuole.

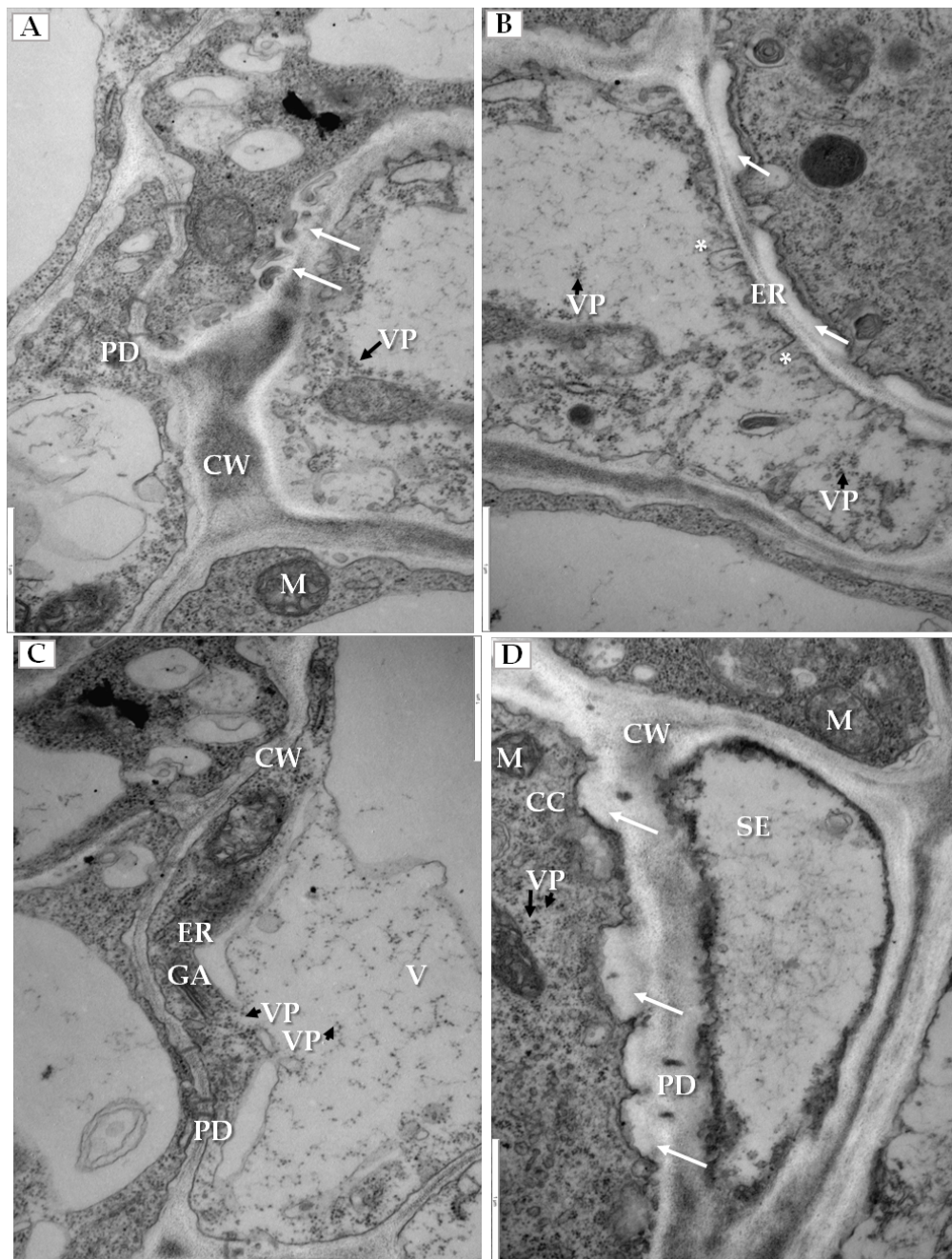


**Figure 7.** Changes in cell wall structure and plasmalemma in phloem cells of PDV infected cucumber leaves. **(A)** Fragment of phloem parenchyma with cell-wall invaginations (white arrow). Viral particles (VP, black arrow) in phloem parenchyma cell, Bar 1  $\mu\text{m}$ ; **(B)** Fragments of phloem parenchyma cells with irregular cell wall (white arrow) and plasmalemma invaginations (\*) and with viral particles (VP, black arrow), Bar 1  $\mu\text{m}$ ; **(C)** Presence of viral particles (VP, black arrow) inside the vacuole with the vacuolar lumen having connections to the cytoplasm of parenchyma cell, Bar 1  $\mu\text{m}$ ; **(D)** An irregular and thicker cell wall (white arrow) between companion cell with viral particles (VP, black arrow) and sieve tube, Bar 1  $\mu\text{m}$ . Abbreviations: CW—cell wall, PD—plasmodesmata, ER—endoplasmic reticulum, GA—Golgi apparatus, MT—movement protein induced tubular structures, VP, black arrow—viral particles, SE—sieve tube, CC—companion cell, M—mitochondrion, V—vacuole.

#### 2.4. Modeling of 3D Structures of PDV-0599 and Alfalfa Mosaic Virus-VRU (AMV-VRU) Movement Proteins (MPs)

Our previous studies and literature data revealed some similarities among the amino-acids of movement protein (MP) of PDV and that of *Alfalfa mosaic virus* (AMV). AMV has a well-described mechanism of cell-to-cell transport or the role of its MP in viral infection. However, the structure of PDV-MP is unknown, whereas the function of MP's amino acids sequence is only one side of coin. The 3D structure of viral MPs in general has a significant influence on function during viral infection and especially on cell-to-cell transport. We compared the structures of MPs of PDV and AMV to clarify similarities between both viruses to better understand their function. The use of Jalview and AIDA server enabled us to distinguish regions with characteristic structure. Apparently, most of the sequence in both MPs formed a simple loop structure. There were different numbers of  $\alpha$ -helical and  $\beta$ -sheet regions in both structures (Figure 8A–D). The MP of PDV-0599 had seven  $\alpha$ -helical (5 short helices-1-3 coils, and 2 longer helices with 5 coils) and eight  $\beta$ -sheet regions (Figure 8A). RBD localized between 56–85 aa in PDV-MP sequence consisted of one loop and two  $\alpha$ -helices. AMV-MP had less number of complex regions (Figure 8) with five  $\alpha$ -helices (4 short helices-1-3 coils and one long helix with 4 coils) and three  $\beta$ -sheets. These regions were localized at equivalent points within the overall protein structure (Figure 8A,C). RBD was also identified between 56–85 aa in AMV-MP, being quite similar to RBD of PDV, except that AMV had only one helical region (Figure 8D). Despite the differences in number of  $\alpha$ -helical and  $\beta$ -sheet regions, an overlay of the 3D structures indicated more similarities than differences between both proteins (Figure 8E).

#### 2.5. Localization and Quantification of PDV-CP and MP in Infected Cucumber Leaves by Double-Immunogold

Local (cell-to-cell) transport could be studied by localizing two major viral proteins, CP and MP in tubular structures that contain virus particles, by using double-immunogold technique. We have co-localized CP and MP in specific parts of infected cell. Both epitopes were detected together inside the tubular structures inside plasmodesmata (Figure 9A), but CP epitope was located on viral particles not only in tubular structures but also in the cytoplasm (Figure 9A,B). Moreover, MP and CP co-localized inside secondary plasmodesmata and in the cytoplasm near plasmodesmata (Figure 9C). No PDV-CP and MP epitopes were detected in mock-inoculated cucumber plants (Figure 9D).

To quantify the co-localization of PDV-CP and MP, the statistical dual labelling was performed. The values of the odds ratio (OR) and the results from Fisher's test for double-immunogold parameters (estimated statistical values  $p < 0.001$ ) revealed that the zero hypothesis—i.e., that localizations of CP and MP are independent of each other—has to be rejected. Positive values of the OR in case of plasmodesmata containing tubular structures (OR = 12.04), cytoplasm (OR = 5.66), and vacuole (OR = 2.40), with a high incidence of double positives coupled with a high incidence of double negatives, indicated the statistically significant co-localization of MP and CP in these cellular compartments (Table 1). Moreover, differences between the OR values showed that the strongest co-localization of PDV-CP and MP was observed in plasmodesmata and in tubular structures. The co-localization level was lower in the cytoplasm and the lowest in the vacuole.

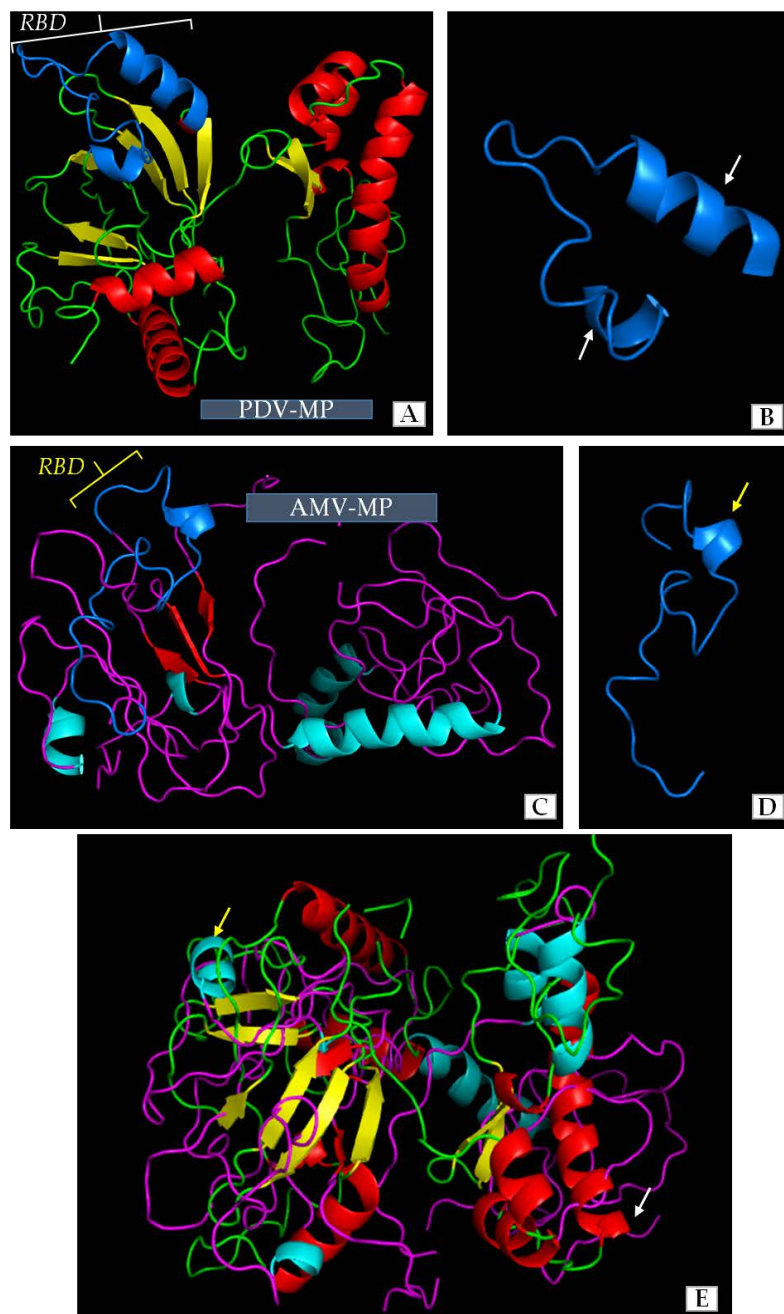


**Figure 8.** Three-dimensional (3D) model structures of the PDV movement protein (PDV-MP) and AMV movement protein (AMV-MP). (A) 3D model of PDV-MP structure. The colors show the particular elements of the secondary structure, as follows. Green indicates the fragments of straight polypeptide chain, red— $\alpha$ -helical fragments, yellow— $\beta$ -card fragments, blue—RNA binding domain (RBD); (B) The blue color represents the RBD structure of PDV-MP, enlarged from (A). White arrows indicate two  $\alpha$ -helical fragments of this domain; (C) 3D model of AMV-MP structure. The colors show the particular elements of the secondary structure as follows. Purple indicates the fragments of straight polypeptide chain, green— $\alpha$ -helical fragments, red— $\beta$ -card fragments, blue—RNA binding domain (RBD); (D) The blue color show RBD structure of AMV-MP enlarged from (C). Yellow arrow specifies the  $\alpha$ -helical fragment of this domain; (E) Overlaid of 3D models of PDV-MP and AMV-MP. Yellow and white arrows show AMV-MP and PDV-MP, respectively. The colors represent the particular elements as shown in (A,C) for PDV-MP and AMV-MP, respectively.

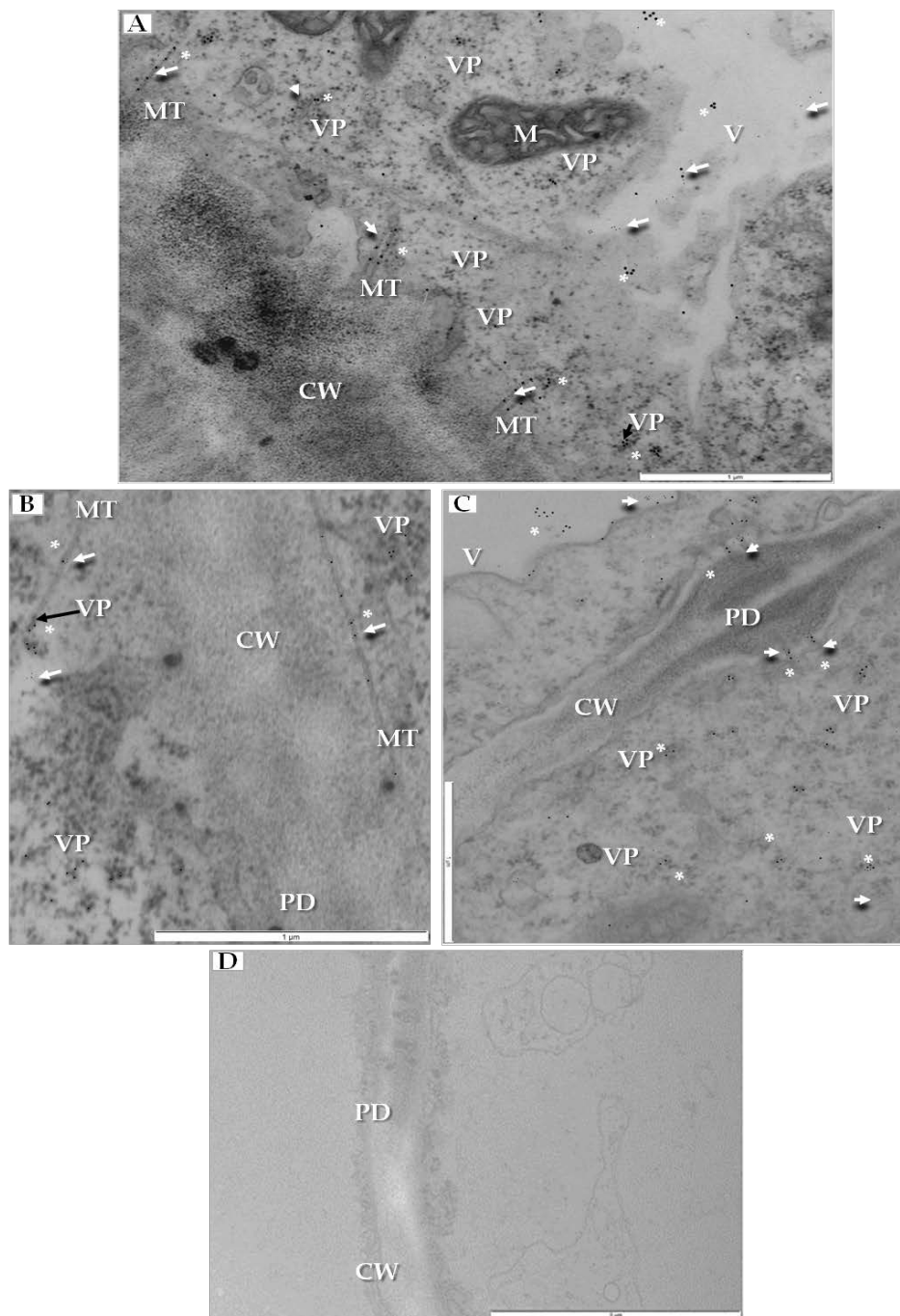


**Figure 9.** Double-immunogold localization of PDV movement protein (MP) and coat protein (CP) in infected cucumber leaf tissues (14 dpi). (A) MP epitopes (white arrow) and CP epitopes (\*) colocalized in tubular structures in plasmodesmata, cytoplasm and vacuole. CP epitopes (\*) on the surface of viral particles. Labeled viral particles in cytoplasm (VP, black arrow), Bar 1 µm; (B) Viral particles (VP, black arrow) in tubular structure. Co-localization of MP epitopes (white arrow) and CP epitopes (\*) are visible, Bar 1 µm; (C) Two types of gold particles (\* and white arrow) from CP and MP co-localized in cytoplasm and in plasmodesma, Bar 1 µm; (D) Fragment of parenchyma cell from mock-inoculated cucumber without MP and CP epitopes, Bar 1 µm. Abbreviations: CW—cell wall, PD—plasmodesmata, M—mitochondrion, V—vacuole, MT—movement protein induced tubular structures, VP—viral particles.

**Table 1.** Quantification of preferential double-immunogold localization of CP and MP in  $2 \times 2$  contingency table from GraphPad Software. (A) Quantification of double-immunolocalization parameters in PDV-infected cucumber leaves. Two-tailed  $p$  value ( $p$ ) for cell segments analyses was less than 0.0001. (B) Quantification of double-immunolocalization parameters in mock-inoculated cucumber leaves. No localization was observed. OR—odds ratio, CP<sub>g20+</sub>—presence of 20 nm gold particles associated with presence of CP epitope, CP<sub>g20-</sub>—absence of 20 nm gold particles associated with presence of CP epitope, MP<sub>g10+</sub>—presence of 10 nm gold particles associated with presence of MP epitope, MP<sub>g10-</sub>—absence of 10 nm gold particles associated with presence of MP epitope. In table bold and red color value is result of statistical analyses of Quantification of preferential double-immunogold localization.

Double-Immunolocalization Parameters				
(A) PDV-infected mesophyll cells:				
-plasmodesmata and tubular structures				
Protein	MP <sub>g10+</sub>	MP <sub>g10-</sub>	Row totals	Ratio MP <sub>g10+</sub> /MP <sub>g10-</sub>
CP <sub>g20+</sub>	47	6	53	7.83
CP <sub>g20-</sub>	13	20	14	0.65
Column totals	60	27	87	<b>OR = 12.04</b>
-cytoplasm				
Protein	MP <sub>g10+</sub>	MP <sub>g10-</sub>	Row totals	Ratio MP <sub>g10+</sub> /MP <sub>g10-</sub>
CP <sub>g20+</sub>	41	24	65	1.7
CP <sub>g20-</sub>	9	30	39	0.3
Column totals	50	54	104	<b>OR = 5.66</b>
-vacuole				
Protein	MP <sub>g10+</sub>	MP <sub>g10-</sub>	Row totals	Ratio MP <sub>g10+</sub> /MP <sub>g10-</sub>
CP <sub>g20+</sub>	20	16	36	1.25
CP <sub>g20-</sub>	12	23	34	0.52
Column totals	32	38	70	<b>OR = 2.40</b>
(B) Mock inoculated mesophyll cells:				
-Plasmodesmata, tubular structures, cytoplasm and vacuole				
Protein	MP <sub>g10+</sub>	MP <sub>g10-</sub>	Row totals	Ratio MP <sub>g10+</sub> /MP <sub>g10-</sub>
CP <sub>g20+</sub>	0	0	0	0
CP <sub>g20-</sub>	0	0	0	0
Column totals	0	0	0	0

### 3. Discussion

In this work we conducted ultrastructural analyzes of PDV-infected tissues in order to address the mechanisms of pathogenesis and virus transportation in cucumber. The results of these studies allowed us to draw several important conclusions. The first group of results regards the morphological changes and symptoms of PDV infection. PDV is present all over the world [1] causing increasing problems in a wide range of plant hosts [3,13], especially in orchard trees from the genus *Prunus* (sweet or sour cherry, plum or peach) [12]. PDV is well propagated by mechanic transmission [14–16], but less importantly by pollen and seeds [8,13,17], and interferes with the vegetative propagation of trees [14–16].

Different strains/isolates of PDV can generate different symptoms in the same host [3,12], causing different plant diseases [7]. Among the effects caused by all PDV strains [3,8], there are dwarfing and reduction in flowers and fruits [13]. Two phases of disease [4] include a “shock” phase observed during first two years [8] followed by the asymptomatic chronic phase [3,8]. During “shock” phase [8,18,19], not only does PDV induces strain-specific chlorotic spots/rings and mottle or line patterns on leaf blades [20–22], but also reduces the growth of shoots [23] or the number of flowers [5]. The flowers remain strongly deformed, without stamens [8,23]. The chronic phase involves growth reduction of plants whereas the concentration of the virus is generally very low, barely detectable by DAS-ELISA [24], best detected between March and May [24]. The PDV disease can easily be overlooked in nurseries [3,13]. Therefore, the presence of PDV is verified on test plants including *Cucumis sativus* (especially cv. Wisconsin and cv. Polan), *Cucurbita maxima* (for example cv. Buttercup) and *Nicotiana tabacum* cv. Samsun [3,4,20,24].

In our experiments, PDV-0599 induced local chlorotic spots on the inoculated cotyledons of *Cucumis sativus* cv. Polan 7 dpi, similar to those presented by Fulton [20]. Moreover, further alteration/deformation and chlorotic lesions of fully developed leaves were observed 14 dpi, as an element of systemic spread, also described by Fulton [20]. Leaf deformations and chlorotic lesions were documented on plums [3,8] or *Nicotiana tabaccum* cv. Samsun. Kozieł [25] noted chlorotic alternations and deformation of the upper side of systemic leaves after 15 dpi, also observed by Waterworth and Fulton [26]. Other members of the *Bromoviridae* family, such as AMV can induce leaf vein necrosis in tobacco leaves, often reaching vascular tissues [27–29].

Cotyledons and fully developed leaves of cucumber have different morphology, with cotyledons retaining some embryonic features in anatomical structure, whereas upper leaves are characteristic for mature plants [30]. The structure of fully developed cucumber leaves is more similar to those of *Prunus* sp. [30]. Therefore, we have used systemically infected cucumber leaves as models for ultrastructural investigations of the effects of PDV in mature plant organs.

Secondly, by using immunofluorescence we localized the PDV-CP epitopes in the cucumber tissue. In general, the PDV-CP can reach much higher levels during viral infection than other PDV proteins [5,31]. Apart from forming viral particles, the CP of *Illarviruses* is engaged in the asymmetric (+)/(-) strand RNA synthesis, translation of viral RNA, and during both intercellular and systemic transport [10]. Previously, using the immunofluorescence and TEM, Kozieł et al. [32] co-localized PDV-CP and the replicase P1 protein, as an efficient marker of ongoing PDV replication. The presence of PDV-CP epitopes in palisade and spongy mesophyll cells at 14 dpi confirmed the virus spread to various tissues of cucumber, which corresponded to deformations in mesophyll cells, also observed in tobacco [32]. However, in contrast to tobacco, we did not observe necrosis in cucumber vascular bundles at 14 dpi, likely reflecting varying reactions of tobacco and cucumber to PDV.

The systemic transport of PDV seems to occur equally in sieve tubes and xylem vessels, as shown by us in tobacco [33]. Similar results were observed in natural hosts. Malinowski and Zawadzka [24] showed that the best materials for PDV diagnostic tests by Double Antibody Sandwich Enzyme-Linked Immunosorbent Assay (DAS-ELISA) were vascular bundles of leaves and shoots, also true for other *Bromoviridae*. AMV-CP localized inside the palisade and spongy mesophylls but not in vascular tissues at 7 dpi in *Nicotiana benthamiana* [34–36] but at 14 dpi the AMV-CP epitopes were located in mesophyll as well as in vascular tissues. The comparisons of CP sequences of PDV and AMV revealed high similarity at selected regions [25], suggesting similarities between infection mechanisms for both viruses.

Other observations of this work concern ultrastructural changes in cucumber cells. One group of ultrastructural changes induced by plant viruses can be classified as directly connected with viral genome replication and/or with viral particle assembly [37,38]. Different membranous structures can form vesicles with single or double membranes, tubules or stacked membranes [38]. Yet the more complex changes are related to plant reactions against infection, such as those associated with the presence of R (resistance) genes and the accumulation of levels of reactive oxygen species (ROS) [39]. In resistant plants, ROS is frequently associated with the hypersensitive response (HR) [40]. Regardless of resistance or susceptibility, ROS often alters mitochondria and chloroplasts. ROS damage of chloroplasts is reflected by chlorotic lesions or leaf discoloration [37,41]. Plant viruses change the expression of plant genes leading to structural deformations. Plasmodesmata (PD) and the cell wall are amongst the highly modified structures [42,43]. For PDs, the host plant tries to block the path to stop the viral cell-to-cell transport [31], e.g., via callose depositions [44]. *Tobacco mosaic virus* (TMV) is known to induce the synthesis of  $\beta$ -1,3-glucanases which degrade callose, preventing the PD blockage [45]. Cell wall changes are not fully explored in plant-virus interactions [41].

Previously, we reported the localization of sites of PDV replication in tobacco [32]. Here, we characterize for the first time the ultrastructural alterations in PDV-infected cucumber. Three major groups of cellular alterations can be distinguished. The first group involves sequential changes in chloroplasts, mitochondria and ER. In early stages, the observed changes did not parallel the

presence of PDV particles, with the electron translucent regions in chloroplasts, reduced cristae in mitochondria and the enlarged ER cisterns. Later, the viral particles were observed while both chloroplasts and mitochondria were more severely damaged, likely because of ROS. ROS is known to induce programmed cell death [37]. Favali and Conti [46] observed electron translucent regions in chloroplasts of bean infected with AMV. Whereas the enlargement of ER is probably due to the high activity in protein synthesis, such as P1 and P2 replicase proteins, virion assembly (CP) or cell-to-cell transport (MP). In fact, our data on the immunogold localization in tobacco showed PDV-CP frequently localizing to the ER [32], also reported for BMV in *N. benthamiana* [9,47]. Moreover, Koziel [25] observed severe damage to chloroplasts and mitochondria in PDV-infected tobacco. Apart from ROS, some changes may result directly from accumulation of viral particles, as shown for AMV accumulating in chloroplasts [46,48,49].

The second group of alterations concerned membranous structures that can serve as markers of viral genome replication [9,50]. In cucumber infected by PDV vesicular spherules were inside the vacuoles of mesophyll and phloem cells, similar to P1 protein in tonoplast of tobacco [32], These spherules serve as ultrastructural evidence for ongoing PDV RNA replication; for BMV such vesicles differentiate from the ER membranes [9,12,47]. Bamunusinghe et al. [51] demonstrated that BMV-induced spherules depend on the BMV CP, with different CP mutations blocking the formation of viral particles whereas other mutations blocked the formation of membranous structures [51]. The AMV replication occurs at tonoplast with P1 and P2 proteins and the AMV RNAs co-localizing [52]. Thus, membrane alterations caused by PDV are more similar to AMV than BMV, both associating with the vacuole. The association of CP with membrane alterations needs further studies for both BMV and PDV; the preliminary data from immunogold localized the PDV epitopes in the vacuole and at the tonoplast [12,32].

The third group of changes included alterations of the cell wall and plasmodesmata. The cell wall was modified mainly in phloem parenchyma with many invaginations and an irregular wall structure. These have also been observed for other plant viruses. For instance, Otulak-Koziel et al. [41] revealed a higher level of pathogenesis-related protein 2 (PR-2) during a compatible infection by necrotic strain of *Potato virus Y* (PVY<sup>NTN</sup>). The hydroxyproline-rich glycoproteins (HRGP) (extensin) were induced, whereas the cellulose synthase catalytic subunit (CesA4) was downregulated.

Proteins for cell wall metabolism are important because they affect the spread of the virus. Analysis of the deposition of CesA4, PR-2 and HRGP within the apoplast and symplast verified their trafficking in potato cell wall in response to PVY<sup>NTN</sup> [41]. For BMV, AMV and *Cowpea chlorotic mottle virus* (CCMV), changes in the size exclusion limit (SEL) of plasmodesmata were reported [53,54], causing considerable increase of the SEL so that the viral transport can occur [53]. Here we confirm the presence of tubular structures containing PDV particles inside plasmodesmata in cucumber, often observed for plant viruses [37]. Similar tubular structures containing viral particles, protruding from the cell surface were reported for protoplasts infected with BMV or AMV [55–60]. Interestingly, the MPs of BMV or AMV were the only proteins needed for tubule induction in protoplasts. We conclude that ultrastructural modifications of plasmodesmata caused by PDV are similar to those of AMV and BMV.

The computer overlay of the 3D models showed some level of similarity between 3D structures of PDV-0599 MP and AMV-VRU MP, as a whole and specifically between the RNA binding domains (RBD). Both MPs were shown to be the most related within the *Bromoviridae* family [11]. Along these lines, Codoñer et al. [61,62] stated that PDV, *Prunus necrotic ringspot virus* (PNRSV) and AMV are phylogenetically related. Moreover, the MPs of PNRSV, BMV or even *Cucumber mosaic virus* (CMV) could replace the function of MP during AMV infection [63,64], implying similar mechanisms of cell to cell transport [3,11]. Numerous contact points have been revealed between 3D structures of MP and CP in PNRSV [62], suggesting that both proteins may interact during infection.

Finally, by using the double-immunogold co-localization we observed strong correlation between PDV CP and MP in the context of cell-to-cell movement. Plant viruses can move cell-to-cell either as RNA-protein complexes (RNP complex) [63–65] or as the entire viral particles. The first mechanism

could be either dependent or independent of CP. The CP independent transport is characteristic for CCMV where CCMV-MP forms a complex with viral RNA while the unbound MP increases the SEL of plasmodesmata [53,66]. With the second mechanism both MP and CP are needed for cell-to-cell transport [67], e.g., for CMV [68], where CMV-MP increases the SEL [69–72] but the virus is transported as an RNP complex consisting of vRNA, MP and CP; the latter stabilizes the complex during delivery to PD [73,74]. The C-terminal basic arm of CP is probably involved in these interactions [68].

When the entire virions are transported, e.g., in the case of AMV [56] or BMV [55,57], both MP and CP are needed for intercellular transfer [75], with the MPs forming tubular structures [56,57] whereas CP on the surface of virions interacts with MP [9]. Our results with PDV showed strong double-immunogold co-localization of CP and MP within the tubular structures of PD, implying the mechanisms comparable to those of AMV and BMV [9,55,56]. However, both the computer modeling of MP and the MP-CP co-localization suggest PDV transport to be more closely related to AMV than to BMV. Whereas the co-localization of PDV-CP and PDV-MP near tonoplast indicates that vacuole is engaged during interaction of both proteins.

## 4. Materials and Methods

### 4.1. Virus Inoculation

To investigate PDV induced pathogenesis, cell-to-cell transport, and immunolocalizations, the test plant *Cucumis sativus* cv. Polan was selected [3,13], as a cultivar very susceptible for a broad range of PDV isolates/strains. The seedlings were mechanically inoculated at a two cotyledon stage (7 days old) with the PDV-0599 suspension in 0.01 M potassium-phosphate buffer containing diethyldithiocarbamic acid (DIECA) [32]. The inoculum was prepared from plum-infected flower buds, obtained from the Institute of Horticulture in Skierniewice, Poland.

### 4.2. Plant Material Preparations for Immunofluorescence and Immunofluorescence Localization of Coat Protein (CP) in Cucumber Leaves

14 days after PDV-0599 infection, fragments of cucumber leaf blades were fixed in paraformaldehyde and embedded butyl-methyl- acrylate resin (BMM). Parameters of fixation and embedding were as previously described by Kozieł et al. [32].

To investigate the presence of PDV in various plant host cells, immunofluorescence localizations of PDV-CP were performed. Cucumber leaves embedded in BMM were cut into 3 µm thick section. Sections were placed on special Poly-L-Lysine slides (Thermo Scientific, Nettetal, Germany) in a drop of distilled water. Slides with sections were then placed for one day on a thermoblock warmed to 45 °C. This procedure attaches and immobilizes the sections on the slides [32]. In the next step slides with cucumber leaf sections were treated and incubated in a series of solutions from acetone (washing resin from section surface), distilled water, phosphate-buffered saline (PBS) (pre-incubation), PBS containing 2% bovine serum albumin (PBS-BSA) (for blocking of non-specific epitopes) and again with PBS (for washing off residual PBS-BSA). The above series of treatments and further dilution of and incubation with antibodies were performed according to the procedure described by Otulak et al. [76], with modification of Kozieł et al. [32]. PBS-washed slides were treated with primary purified rabbit polyclonal antibody anti-CP-PDV (Bioreba, Reinach, Switzerland). Four rinses in 0.01 M PBS buffer with 0.05% Tween 20, and then one rinse in 0.01 M PBS were applied. The slides were then treated with secondary anti-rabbit antibody IgG with attached AlexaFluor®488 (Jackson Immuno Research Europe Ltd., Cambridgeshire, UK) for 1 h in the dark. After incubation, the sections were washed by PBS-Tween and PBS and stained by DAPI (4', 6-diamidino-2-phenylindole). Immuno-stained sections were imaged in a AX70 PROVIS fluorescent microscope with Olympus UP90 HD camera (Olympus, Warsaw, Poland). Images were acquired using Olympus Cell Sense Standard Software (Olympus, Center Valley, PA, USA, version 1.18).

#### 4.3. Preparation of Plant Material for Transmission Electron Microscopy (TEM) and Double-Immunogold Localization of CP and MP

14 days after PDV inoculation, fragments of leaf blades with symptoms of infection and mock-inoculated (healthy) plants were cut [76,77]. Samples of leaf blades were fixed and then embedded in EPOXY resin according to the procedure described in ref. [78], with modification in Koziel et al. [32]. Then samples in EPOXY resin were cut into ultrathin sections (100 nm) and mounted on copper (for ultrastructural analyses) or nickel grids (for double-immunogold localization) [76–78].

#### 4.4. Comparative Analyses of 3D Models of PDV-0599 and AMV-VRU

To investigate the potential role of PDV-0599 MP in plasmodesmata changes that we observed in cucumber leaf, we performed some bioinformatics analyses. From previously published data, we were aware that amino acid sequences of MP protein were most similar to sequence of Alfalfa mosaic virus-VRU (AMV-VRU, GeneBank: AAD04692.1) [11]. The amino acid sequences of MPs of PDV-0599 and AMV-VRU were taken from NCBI Protein database [79]. and the secondary structures were analyzed with Jalview Desktop 2.10.3b.1. (University of Dundee, Dundee, Scotland) [80]. The 3D structures of whole MPs for both viruses were predicted on AIDA Server (San Diego, CA, USA) [81], according Koziel et al. [32] whereas the most important region of PDV and AMV MPs was compared based on RBD (RNA binding domain). To compare the whole 3D structures and RBDs, the number, type and dimensional localization of structural regions were analyzed. Visualization of MP 3D structure was prepared in PyMOL 2.1.0 (Cambridge, UK) [82].

#### 4.5. Double-Immunogold Localization and Quantification of PDV-CP and MP in Cucumber Leaves

Double-immunogold localization of PDV-CP and MP was performed in addition to the single-immunofluorescent localization of CP. Two sets of antibodies were used. The first set consisted of primary rabbit polyclonal antibody anti-PDV-CP (Bioreba, Switzerland), which targets the whole spectrum of PDV strains, whereas the secondary polyclonal anti-rabbit antibody coupled with colloidal gold (20 nm gold particles) was from Sigma Aldrich, Warsaw, Poland. As the second set, a primary mouse polyclonal antibody PDV-MP (detecting fragment TKGKSSLENVKEAESVH of MP) (GeneCust, Ellange, Luxemburg) PDV-0599 (GeneBank: ADG65215.1) and secondary anti-mouse antibodies coupled to 10nm gold particles (Sigma Aldrich, Warsaw, Poland) were used. The embedded plant material (see above TEM section) was cut on an ultramicrotome to the 100 nm sections (100 nm, placed on nickel grids and treated, as described in refs. [32,77]. Then, the grids were washed in 0.01 M PBS-Tween 20 and PBS, incubated for one hour with the primary antibody rabbit anti-CP-PDV, at a dilution as in Koziel et al. [32]. After incubation, grids were washed in PBS-Tween 20 followed by PBS. The grids were incubated with secondary anti-rabbit IgG conjugated with colloidal gold (20 nm) for 1 h, (dilution as in [32]). After this, incubation grids were washed with PBS-Tween 20 and PBS, incubated with primary mouse polyclonal antibody PDV-MP (at a 1:100 dilution) in PBS, washed in PBS-Tween 20 and PBS, and finally incubated with secondary anti-mouse antibodies associated with 10nm gold particles. Lastly, the grids were rinsed, stained with uranyl acetate and observed in transmission electron microscopy [78]. Double-immunogold colocalization of CP and MP was analyzed using a  $2 \times 2$  contingency table as described by Mayhew [83]. Assessment of in  $2 \times 2$  contingency table was performed separately for all different cell structures including plasmodesmata and tubular structures, cytoplasm and vacuole with the GraphPad Software [84], using the Fisher's exact test. For a more extensive analysis, we also performed an odds ratio (OR) calculation as it was described by Mayhew and Lucocq [85].

## 5. Conclusions

Studies on pathogenic changes during viral plant-pathogen interactions are being conducted at different levels, from the whole-organ morphology to the tissues, cells and subcellular organelles, and the analyzes of cell structures have become increasingly common. These investigations show a range and complexity of pathogenesis during viral infection. PDV is an interesting and extremely damaging viral pathogen, distributed worldwide. Our multifaceted study combines the computer-assisted methods with the ultrastructural observations and the immunolocalization of CP and MP PDV proteins in order to better understand the pathogenesis and cell-to-cell transport of this virus. TEM ultrastructural analyses show the involvement of specific organelles including vacuole, ER, chloroplasts, and mitochondria in the PDV-infected cucumber tissue. PDV infection leads to sequential alterations in the infected cells. All results indicate that intercellular transport of PDV is similar to related *Bromoviridae* BMV and AMV.

**Author Contributions:** E.K. and K.O.-K. wrote the manuscript, conceived the idea of research and performed all experiments; J.J.B. analyzed the data and actively participated in the manuscript preparing.

**Funding:** The work has been supported by Warsaw University of Life Sciences-SGGW grant number: 505-10-011100-Q00190-99

**Acknowledgments:** Authors would like to thank very much to Jens Tilsner, from School of Biology of University of St Andrews (UK) for critical reading/comments and language editing of manuscript.

**Conflicts of Interest:** The authors declare no conflict of interest.

## References

1. Bujarski, J.J.; Figlerowicz, M.; Gallitelli, D.; Roossinck, M.J.; Scott, S.W. Family *Bromoviridae*. In *Virus Taxonomy: Classification and Nomenclature of Viruses-Ninth Report of the International Committee on Taxonomy of Viruses*, 1st ed.; King, A.M.Q., Adams, M.J., Carstens, E.B., Lefkowitz, E.J., Eds.; Elsevier Academic Press: San Diego, CA, USA, 2012; pp. 972–976. ISBN 978-0123846846.
2. Brunt, H.A.; Crabtree, K.; Dallwitz, M.J.; Gibbs, A.J.; Watson, L. *Viruses of Plants*, 1st ed.; CAB International UK: Wallingford, UK, 1996; ISBN 978-0851987941.
3. Paduch-Cichal, E. Characterization of PNRSV and PDV. Associate Professor Thesis, Warsaw University of Life Sciences, Warsaw, Poland, 2000.
4. Fulton, R.W. *Prune dwarf virus*. *C.M.I./A.A.B. Descr. Plant Viruses* **1970**, *1*.
5. Pallas, V.; Aparicio, F.; Herranz, M.C.; Amari, K.; Sanchez-Pina, M.A.; Myrta, A.; Sanchez-Navarro, J.A. *Iilarviruses of Prunus spp.: A continued concern for fruit trees*. *Phytopathology* **2012**, *102*, 1108–1120. [[CrossRef](#)] [[PubMed](#)]
6. Pallas, V.; Aparicio, F.; Herranz, M.C.; Sanchez-Navarro, J.A.; Scott, S.W. The molecular biology of ilarviruses. *Adv. Virus Res.* **2013**, *87*, 139–183. [[CrossRef](#)] [[PubMed](#)]
7. Kalinowska, E.; Mroczkowska, K.; Paduch-Cichal, E.; Chodorska, M. Genetic variability among coat protein of *Prune dwarf virus* variants from different countries and different *Prunus* species. *Eur. J. Plant Pathol.* **2014**, *4*, 863–868. [[CrossRef](#)]
8. Nemeth, M. *Virus, Mycoplasma and Rickettsia Diseases of Fruit Trees*, 1st ed.; Springer: Budapest, Hungary, 1986; pp. 600–650. ISBN 978-90-247-2868-8.
9. Sztuba-Solińska, J.; Bujarski, J.J. Insights into the single-cell reproduction cycle of members of the family *Bromoviridae*: Lessons from the use of protoplast systems. *J. Virol.* **2008**, *82*, 10330–10340. [[CrossRef](#)] [[PubMed](#)]
10. Bol, J.F. Replication of alfamo- and ilarviruses: Role of the coat protein. *Annu. Rev. Phytopathol.* **2005**, *43*, 39–62. [[CrossRef](#)] [[PubMed](#)]
11. Kozieł, E.; Otulak, K.; Garbaczewska, G. Phylogenetic analysis of PDV movement protein compared to *Bromoviridae* members as justification of possible intercellular movement. *Acta Biol. Crac. Ser. Bot.* **2015**, *57*, 19–31. [[CrossRef](#)]
12. Kozieł, E.; Bujarski, J.J.; Otulak, K. Molecular biology of *Prune Dwarf Virus*—A lesser known member of the *Bromoviridae* but a vital component in the dynamic virus–host cell interaction network. *Int. J. Mol. Sci.* **2017**, *18*, 2733. [[CrossRef](#)] [[PubMed](#)]

13. Paduch-Cichal, E.; Sala-Rejczak, K. Biological properties, stability in crude sap and serological characterization of *Prune dwarf virus* (PDV) isolates from *Prunus avium* seedlings. *Phytopathol. Pol.* **2003**, *29*, 9–22.
14. Boulila, M. Molecular characterization of an almond isolate of *Prune dwarf virus* in Tunisia: Putative recombination breakpoints in the partial sequences of the coat protein-encoding gene in isolates from different geographic origin. *Phytopathol. Mediterr.* **2009**, *48*, 411–421. [[CrossRef](#)]
15. Öztürk, Y.; Çevik, B. Genetic Diversity in the coat rotein genes of *Prune dwarf virus* isolates from sweet cherry growing in Turkey. *Plant Pathol. J.* **2015**, *31*, 41–49. [[CrossRef](#)] [[PubMed](#)]
16. Kinoti, W.M.; Constable, F.E.; Nancarrow, N.; Plummer, K.M.; Rodoni, B. The incidence and genetic diversity of *Apple mosaic virus* (ApMV) and *Prune dwarf virus* (PDV) *Prunus* species in Australia. *Viruses* **2018**, *10*, 136. [[CrossRef](#)] [[PubMed](#)]
17. Nemeth, M. Interferencja vizsgálato k a csonthéjas gyümöcsfák gyürüsoltosság (ringspot) virusavial. *Növényvédelem* **1972**, *8*, 64–71.
18. Myrta, A.; Savino, V. Virus and virus-like diseases of cherry in the Mediterranean region. *Acta Hort.* **2008**, *795*, 891–896. [[CrossRef](#)]
19. Çağlayan, K.; Gazel, M. Virus and virus-like diseases of stone fruits in the eastern Mediterranean area of Turkey. *Acta Hort.* **1998**, *472*, 527–529. [[CrossRef](#)]
20. Fulton, R.W. Comparative host ranges of certain mechanically transmitted viruses of *Prunus*. *Phytopatology* **1957**, *47*, 215–220.
21. Halk, R.; Fulton, R.W. Stabilization and particle morphology of *Prune dwarf virus*. *Virology* **1978**, *91*, 434–443. [[CrossRef](#)]
22. Fulton, R.W. Purification of Sour cherry necrotic ringspot and *Prune dwarf viruses*. *Virology* **1959**, *9*, 522–535. [[CrossRef](#)]
23. Cropley, R.; Gilmer, R.M.; Posnette, A.F. Necrotic ring spot and *Prune dwarf viruses* in *Prunus* and in herbaceous indicators. *Ann. Appl. Biol.* **1964**, *53*, 325–332. [[CrossRef](#)]
24. Malinowski, T.; Zawadzka, B. Use of ELISA method in detection of fruit trees viruses. In Proceedings of the XXXIII Poland Pomology Conference, Skierniewice, Poland, 30 August–1 September 1994; The Research Institute of Pomology: Skierniewice, Poland, 1994; pp. 9–11.
25. Kozieł, E. Pathogenic Changes in Vegetative Organs of Plum Tree and Test Plants Infected by *Prune Dwarf Virus* (PDV). Ph.D. Thesis, Warsaw University of Life Sciences, Warsaw, Poland, 2016.
26. Waterworth, H.E.; Fulton, R.W. Variation among isolates of necrotic ringspot and *Prune dwarf viruses* isolated from sour cherry. *Phytopathology* **1964**, *54*, 1155–1160.
27. Zaumayer, W.J. Alfalfa yellow mosaic virus systemically infectious to beans. *Phytopathology* **1953**, *43*, 38–42.
28. Zaumayer, W.J. Two new strains of *Alfalfa mosaic virus* systemically infectious to bean. *Phytopathology* **1963**, *53*, 444–449.
29. Zaumayer, W.J.; Patino, G. Vein Necrosis, another systemically infectious strain of *Alfalfa mosaic virus* in bean. *Phytopathology* **1960**, *50*, 226–231.
30. Buchanan, B.B.; Gruissem, W.; Jones, R.L. *Biochemistry and Molecular Biology of Plants*, 2nd ed.; Wiley-Blackwell: New York, NY, USA, 2015; pp. 984–1040. ISBN 978-0-470-71421-8.
31. Schoelz, J.E.; Harries, P.A.; Nelson, R.S. Intracellular transport of plant viruses: Finding the door out of the cell. *Mol. Plant* **2011**, *4*, 813–831. [[CrossRef](#)] [[PubMed](#)]
32. Kozieł, E.; Otulak, K.; Lockhart, B.E.L.; Garbaczewska, G. Subcellular localization of proteins associated with *Prune dwarf virus* replication. *Eur. J. Plant Pathol.* **2017**, *149*, 653–668. [[CrossRef](#)]
33. Mochizuki, T.; Nobuhara, S.; Nishimura, M.; Ryang, B.S.; Naoe, M.; Matsumoto, T.; Kosaka, Y.; Ohki, S.T. The entry of *Cucumber mosaic virus* into cucumber xylem is facilitated by co-infection with Zucchini yellow mosaic virus. *Arch. Virol.* **2016**, *161*, 2683–2692. [[CrossRef](#)] [[PubMed](#)]
34. Van Pelt-Heerschap, H.; Verbeek, H.; Huisman, M.J.; Loesch-Fries, L.S.; Van Vloten-Doting, L. Non-structural proteins and RNAs of *Alfalfa mosaic virus* synthesized in tobacco and cowpea protoplasts. *Virology* **1987**, *161*, 190–197. [[CrossRef](#)]
35. Van Pelt-Heerschap, H. Immunochemical Analysis of the *Alfalfa mosaic virus* Gene Products. Ph.D. Thesis, Leiden University, Leiden, The Netherlands, 1987.
36. Van der Kuyl, A.C.; Neeleman, L.; Bol, J.F. Deletion analysis of cis and trans acting elements involved in the replication of alfalfa mosaic virus RNA 3 in vivo. *Virology* **1991**, *183*, 687–694. [[CrossRef](#)]
37. Hull, R. *Plant Virology*, 5th ed.; Elsevier Academic Press: London, UK, 2013; pp. 148–603. ISBN 9780123848710.

38. Matthews, R.E.F. *Plant Virology*, 3th ed.; Elsevier Academic Press: London, UK, 1991; pp. 143–519. ISBN 978-0-12-480553-8.
39. Dangl, J.L.; Dietrich, R.A.; Richberg, M.H. Death don't have no mercy: Cell death programs in plant-microbe interactions. *Plant Cell* **1996**, *8*, 1793–1807. [[CrossRef](#)] [[PubMed](#)]
40. Chikh Ali, M.; Karasev, A.V.; Furutani, N.; Taniguchi, M.; Kano, Y.; Sato, M.; Natsuaki, T.; Maoka, T. Occurrence of Potato virus Y strain PVY NTN in foundation seed potatoes in Japan, and screening for symptoms in Japanese potato cultivars. *Plant Pathol.* **2013**, *62*, 1157–1165. [[CrossRef](#)]
41. Otulak-Kozieł, K.; Kozieł, E.; Lockhart, B.E.L. Plant cell wall dynamics in compatible and incompatible potato response to infection caused by Potato virus Y (PVY<sup>NTN</sup>). *Int. J. Mol. Sci.* **2018**, *19*, 862. [[CrossRef](#)] [[PubMed](#)]
42. Alexander, M.M.; Cilia, M. A molecular tug-of-war: Global plant proteome changes during viral infection. *Curr. Plant Biol.* **2016**, *5*, 13–24. [[CrossRef](#)]
43. Di Carli, M.; Benvenuto, E.; Donini, M. Recent insights into plant–virus interactions through proteomic analysis. *J. Proteome Res.* **2012**, *11*, 4765–4780. [[CrossRef](#)] [[PubMed](#)]
44. Bruknard, J.O.; Zambryski, P.C. Plasmodesmata enable multicellularity: New insights into their evolution, biogenesis, and functions in development and immunity. *Curr. Opin. Plant Biol.* **2017**, *35*, 76–83. [[CrossRef](#)]
45. Bucher, G.L.; Tarina, C.; Heinlein, M.; Di Serio, F.; Meins, F., Jr.; Iglesias, V.A. Local expression of enzymatically active class I beta-1,3-glucanase enhances symptoms of TMV infection in tobacco. *Plant J.* **2001**, *28*, 361–369. [[CrossRef](#)] [[PubMed](#)]
46. Favali, M.A.; Conti, G.G. Ultrastructural observations on the chloroplasts of basil plants either infected with different viruses or treated with 3-amino-1,2,4-triazole. *Protoplasma* **1970**, *70*, 153–166. [[CrossRef](#)]
47. Bamunusinghe, D.; Seo, J.K.; Rao, A.L. Subcellular localization and rearrangement of endoplasmic reticulum by Brome mosaic virus capsid protein. *J. Virol.* **2011**, *85*, 2953–2963. [[CrossRef](#)] [[PubMed](#)]
48. Hull, R.; Hills, G.J.; Markham, R. Studies on *Alfalfa mosaic virus*: II. The structure of the virus components. *Virology* **1969**, *37*, 416–428. [[CrossRef](#)]
49. Hull, R.; Rees, M.W.; Short, M.N. Studies on *Alfalfa mosaic virus*: I. The protein and nucleic acid. *Virology* **1969**, *37*, 404–415. [[CrossRef](#)]
50. Verchot, J. Wrapping membranes around plant virus infection. *Curr. Opin. Virol.* **2011**, *1*, 388–395. [[CrossRef](#)] [[PubMed](#)]
51. Bamunusinghe, D.; Chaturvedi, S.; Seo, J.K.; Rao, A.L. Mutations in the capsid protein of Brome mosaic virus affecting encapsidation eliminate vesicle induction in planta: Implications for virus cell-to-cell spread. *J. Virol.* **2013**, *87*, 8982–8992. [[CrossRef](#)] [[PubMed](#)]
52. Ibrahim, A.; Hutchens, H.M.; Berg, R.H.; Loesch-Fries, S. *Alfalfa mosaic virus* replicase proteins, P1 and P2, localize to the tonoplast in the presence of virus RNA. *Virology* **2012**, *433*, 449–461. [[CrossRef](#)] [[PubMed](#)]
53. Rao, A.L.N. Molecular studies on Bromovirus capsid protein. III. Analysis of cell-to-cell movement competence of coat protein defective variants of cowpea chlorotic mottle virus. *Virology* **1997**, *232*, 385–395. [[CrossRef](#)] [[PubMed](#)]
54. Sanchez-Navarro, J.A.; Herranz, M.C.; Pallas, V. Cell-to-cell movement of *Alfalfa mosaic virus* can be mediated by the movement proteins of Ilar-, bromo-, cucumo-, tobamo- and comoviruses and does not require virion formation. *Virology* **2006**, *346*, 66–73. [[CrossRef](#)] [[PubMed](#)]
55. Flasiński, S.; Dzianott, A.; Pratt, S.; Bujarski, J. Mutational analysis of coat protein gene of brome mosaic virus: Effects on replication and movement protein in barley and on *Chenopodium hybridum*. *Mol. Plant Microbe Interact.* **1995**, *8*, 23–31. [[CrossRef](#)] [[PubMed](#)]
56. Rao, A.L.; Grantham, G.L. Biological significance of the seven amino-terminal basic residues of brome mosaic virus coat protein. *Virology* **1995**, *211*, 42–52. [[CrossRef](#)] [[PubMed](#)]
57. Van der Vossen, E.A.; Neeleman, L.; Bol, J.F. Early and late functions of *Alfalfa mosaic virus* coat protein can be mutated separately. *Virology* **1994**, *202*, 891–903. [[CrossRef](#)] [[PubMed](#)]
58. Van der Wel, N.N.; Goldbach, R.W.; van Lent, J. The movement protein and coat protein of *Alfalfa mosaic virus* accumulate in structurally modified plasmodesmata. *Virology* **1998**, *244*, 322–329. [[CrossRef](#)] [[PubMed](#)]
59. Kaido, M.; Inoue, Y.; Takeda, Y.; Sugiyama, K.; Takeda, A.; Mori, M.; Tamai, A.; Meshi, T.; Okuno, T.; Mise, K. Downregulation of the *NbNACA1* gene encoding a movement-protein-interacting protein reduces cell-to-cell movement of brome mosaic virus in *Nicotiana benthamiana*. *Mol. Plant Microbe Interact.* **2007**, *20*, 671–681. [[CrossRef](#)] [[PubMed](#)]

60. Kasteel, D.T.J.; van der Wel, N.N.; Jansen, K.A.J.; Goldbach, R.W.; van Lent, J.W.M. Tubule-forming capacity of the movement proteins of *Alfalfa mosaic virus* and brome mosaic virus. *J. Gen. Virol.* **1997**, *78*, 2089–2093. [CrossRef] [PubMed]
61. Codoñer, F.M.; Cuevas, J.M.; Sánchez-Navarro, J.A.; Pallas, V.; Elena, S.F. Molecular evolution of the plant virus family *Bromoviridae* based on RNA3-encoded proteins. *J. Mol. Evol.* **2005**, *61*, 697–705. [CrossRef] [PubMed]
62. Codoñer, F.M.; Fares, M.A.; Elena, S.F. Adaptive covariation between the coat and movement proteins of *Prunus necrotic ringspot virus*. *J. Virol.* **2006**, *80*, 5833–5840. [CrossRef] [PubMed]
63. International Committee on Taxonomy of Viruses (ICTV) Official Website. Available online: [https://talk.ictvonline.org/ictv-reports/ictv\\_9th\\_report/positive-sense-rna-viruses-2011/w/posrna\\_viruses/251/bromoviridae](https://talk.ictvonline.org/ictv-reports/ictv_9th_report/positive-sense-rna-viruses-2011/w/posrna_viruses/251/bromoviridae) (accessed on 16 April 2018).
64. Tomenius, K.; Clapham, D.; Meshi, T. Localization by immunogold cytochemistry of the virus coded 30K protein in plasmodesmata of leaves infected with tobacco mosaic virus. *Virology* **1987**, *160*, 363–371. [CrossRef]
65. Lucas, W.J.; Ding, B.; Van der Schoot, C. Plasmodesmata and the supracellular nature of plants. *New Phytol.* **1993**, *125*, 435–476. [CrossRef]
66. Herranz, M.C.; Sanchez-Navarro, J.A.; Sauri, A.; Mingarro, I.; Pallas, V. Mutational analysis of the RNA-binding domain of the prunus necrotic ringspot virus (PNRSV) movement protein reveals its requirement for cell-to-cell movement. *Virology* **2005**, *339*, 31–41. [CrossRef] [PubMed]
67. Kaplan, I.B.; Zhang, L.; Palukaitis, P. Characterization of Cucumber mosaic virus: Cell to cell movement requires capsid protein but not virions. *Virology* **1998**, *246*, 221–231. [CrossRef] [PubMed]
68. Schmitz, I.; Rao, A.L.N. Deletions in the conserved amino-terminal basic arm of cucumber mosaic virus coat protein disrupt virion assembly but do not abolish infectivity and cell-to-cell movement. *Virology* **1998**, *248*, 323–331. [CrossRef] [PubMed]
69. Suzuki, M.; Kuwata, S.; Kataoka, J.; Masuta, C.; Nitta, N.; Takanami, Y. Functional analysis of deletion mutants of Cucumber mosaic virus RNA3 using an in vitro transcription system. *Virology* **1991**, *183*, 106–113. [CrossRef]
70. Canto, T.; Prior, D.A.M.; Hellwald, K.H.; Oparka, K.J.; Palukaitis, P. Characterization of Cucumber mosaic virus. IV. Movement protein and coat protein are both essential for cell-to-cell movement of CMV. *Virology* **1997**, *237*, 237–248. [CrossRef] [PubMed]
71. Kaplan, I.B.; Gal-On, A.; Palukaitis, P. Characterization of Cucumber mosaic virus. III. Localization of sequences in the movement protein controlling systemic infection in cucurbits. *Virology* **1997**, *230*, 343–349. [CrossRef] [PubMed]
72. Canto, T.; Palukaitis, P. Are tubules generated by the 3a protein necessary for cucumber mosaic virus movement? *Mol. Plant Microbe Interact.* **1999**, *12*, 985–993. [CrossRef]
73. Lucas, W. Plant viral movement proteins: Agents for cell-to-cell trafficking of viral genomes. *Virology* **2006**, *344*, 169–184. [CrossRef] [PubMed]
74. Li, Q.B.; Palukaitis, P. Comparison of the nucleic acid- and NTP-binding properties of the movement protein of cucumber mosaic cucumovirus and tobacco mosaic tobamovirus. *Virology* **1996**, *216*, 71–79. [CrossRef] [PubMed]
75. Okinaka, Y.; Mise, K.; Suzuki, E.; Okuno, T.; Furusawa, I. The C terminus of brome mosaic virus coat protein controls viral cell-to-cell and long-distance movement. *J. Virol.* **2001**, *75*, 5385–5390. [CrossRef] [PubMed]
76. Otulak, K.; Kozieł, E.; Lockhart, B.E.L.; Garbaczewska, G. Ultrastructural effects of PVY<sup>NTN</sup> infection of *Capsicum annuum* L. cv. Yolo Wonder generative organs; a first step in describing seed transmission. *Phytopathol. Mediterr.* **2017**, *56*, 379–391. [CrossRef]
77. Otulak, K.; Garbaczewska, G. Ultrastructural events during hypersensitive response of potato cv. Rywal infected with necrotic strains of potato virus Y. *Acta Physiol. Plant.* **2010**, *32*, 635–644. [CrossRef]
78. Hayat, M. *Basic Techniques for Transmission Electron Microscopy*, 1st ed.; Elsevier Academic Press International: San Diego, CA, USA, 1986; pp. 285–370. ISBN 978-0-12-333926-3.
79. NCBI Protein Database Official Website. Available online: <https://www.ncbi.nlm.nih.gov/protein/> (accessed on 28 April 2018).
80. Jalview Official website. Available online: <http://www.jalview.org/> (accessed on 28 April 2018).
81. AIDA Server Official Website. Available online: <http://aida.godziklab.org/AIDA/> (accessed on 28 April 2018).

82. PyMOL Official Website. Available online: <https://pymol.org/2/> (accessed on 28 April 2018).
83. Mayhew, T.M. Quantifying immunogold localization on electron microscopic thin sections: A compendium of new approaches for plant cell biologists. *J. Exp. Bot.* **2011**, *62*, 4101–4113. [[CrossRef](#)] [[PubMed](#)]
84. GraphPad Software Official Website. Available online: <https://www.graphpad.com/quickcalcs/contingency1.cfm> (accessed on 28 April 2018).
85. Mayhew, T.M.; Lucocq, J.M. Multiple-labelling immunoEM using different sizes of colloidal gold: Alternative approaches to test for differential distribution and colocalization in subcellular structures. *Histochem. Cell Biol.* **2011**, *135*, 317–326. [[CrossRef](#)] [[PubMed](#)]



© 2018 by the authors. Licensee MDPI, Basel, Switzerland. This article is an open access article distributed under the terms and conditions of the Creative Commons Attribution (CC BY) license (<http://creativecommons.org/licenses/by/4.0/>).